Explicit Finite-Difference and Particle Method for the Dynamics of Mixed Bose-Condensate and Cold-Atom Clouds

P. Vignolo,* M. L. Chiofalo,* M. P. Tosi,* and Sauro Succi†

*INFM and Classe di Scienze, Scuola Normale Superiore, Piazza dei Cavalieri 7, I-56126 Pisa, Italy;
and †Istituto Applicazioni Calcolo CNR "M. Picone" and INFM Roma,
Viale del Policlinico 137, I-00161 Roma, Italy

We present a new numerical method for studying the dynamics of quantum fluids composed of a Bose–Einstein condensate and a cloud of bosonic or fermionic atoms in a mean-field approximation. The method combines an explicit time-marching algorithm, previously developed for Bose–Einstein condensates in a harmonic or optical-lattice potential, with a particle-in-cell approach to the equation of motion for the one-body Wigner distribution function in the cold-atom cloud. The method is tested against known analytical results on the free expansion of a fermion cloud from a cylindrical harmonic trap and is validated by examining how the expansion of the fermionic cloud is affected by the simultaneous expansion of a condensate. We then present original calculations on a condensate and a thermal cloud inside a harmonic well and a superposed optical lattice, by addressing the free expansion of the two components and their oscillations under an applied harmonic force. These results are discussed in the light of relevant theories and experiments.   © 2002 Elsevier Science (USA)

Key Words: Bose–Einstein condensation; finite-difference and particle methods.

I. INTRODUCTION

The physics of ultracold atomic vapors under magnetic or optical confinement has been a continuing and ever expanding focus of interest since the realization of Bose–Einstein condensation [1]. Following characterizations of the basic thermodynamic and dynamical properties of condensates [2], a number of experiments have been performed to investigate their phase coherence and superfluidity [3], to study nonlinear effects and special spectroscopic features [4], and to observe vortices [5]. Parallel efforts are being made in the study of gases of fermionic atoms [6] and of boson–fermion mixtures [7], with the ultimate aim of realizing novel superfluids.

Theoretical studies of the dynamics of these systems, involving the analytical solution of approximate models, have very often been successful in explaining or predicting such novel phenomena. However, the interplay of different species and the thermal fluctuations of a condensate are not easily handled by analytical methods. The validity of the approximations may be limited to the extreme collisionless or hydrodynamic regimes, with the confinement of the sample being treated within a local-density approach. Thus, while the equations governing these dilute systems remain simple, their numerical solution can be helpful for investigating more complex dynamical problems where an intermediate regime is met or a cold-atom cloud accompanies the condensate.

The atomic interactions in a highly dilute Bose gas at very low temperatures, relevant for current experiments, are described by a contact pseudopotential accounting for *s*-wave scattering in binary atom–atom elastic collisions. A condensate is then treated within a mean-field approach by solving the stationary or the time-dependent Gross–Pitaevskii equation (GPE). Several types of numerical approaches have been developed: eigenvalue solvers [8], variational solvers [9], or explicit solvers [10] for the ground state and implicit [11] or explicit [12] time-marching schemes for the dynamics.

Methods for studying the dynamics of an isolated cloud of ultracold (bosonic or fermionic) atoms are also well developed. One needs to solve the Vlasov–Landau equation of motion (VLE) for the Wigner distribution function. Various numerical techniques have been used for this purpose; these are based either on an ergodic assumption [13] or on the inclusion of statistical noise [14], or else they use direct simulation Monte Carlo (DSMC) and related particle-dynamics approaches [15–17].

The general theoretical background is provided by the book of Kadanoff and Baym [18]. These authors developed a Green's function approach to transport phenomena, which extends the Boltzmann equation to strongly interacting quantum fluids and allows for progressively improved self-consistent approximations. This formalism was extended to a homogeneous Bose-condensed gas at finite temperature by Kane and Kadanoff [19], within a Beliaev approximation including interactions up to second order. More recently, these methods have been adapted to the theory of transport phenomena in a confined Bose gas within the Hartree–Fock–Bogoliubov approximation [20, 22, 23], dealing with a Bose–Einstein condensate accompanied by its thermal cloud. Jackson and Adams [24] have proposed to combine the GPE with a quantum version of the DSMC to numerically evaluate the dynamics of such a fluid. Numerical studies based on a generalized GPE combined with a semiclassical kinetic equation, and including collisions between the condensate and the thermal cloud, are also becoming available for dynamical properties of a trapped Bose-condensed gas at finite temperature [25].

In the present work we proceed along the path traced by Jackson and Adams [24]. We propose a different approach to the solution of the GPE and a different method for preparing the initial equilibrium state, which would be immediately applicable to a multicomponent cold-atom cloud. The method is applied to two classes of dynamical problems: The first concerns the ballistic expansion of a fermion cloud and the role played by the presence of a condensate, while the second concerns a Bose-condensed gas in a periodic optical-lattice potential at finite temperature.

After introducing in Section II the model for both the equilibrium state and the dynamical evolution of the fluid, we describe in Section III the numerical methods that we have used to consistently solve the GPE for the condensate and the VLE for the Wigner distribution function of the cloud. The procedure followed in the actual computations is also outlined

in Section III, with due emphasis on the preparation of the initial equilibrium state. The physical applications that we have carried out are presented and discussed in Section IV. A discussion of computational aspects in Section V and some final remarks in Section VI conclude the paper.

II. THE MODEL: A REVIEW OF THE MAIN CONCEPTS

A. *Transport in a Normal Quantum Fluid*

In the original formulation by Kadanoff and Baym (KB), the problem of transport in a quantum fluid in the normal state is tackled by deriving an analogue of the Boltzmann equation for the Wigner distribution function $f(\mathbf{p}, \mathbf{r}, t)$ from the microscopic equations of motion for the nonequilibrium density matrix $\rho(\mathbf{r}_1, t_1; \mathbf{r}_{1'} t_{1'}) \equiv \langle \psi_{\mathcal{U}}^{\dagger}(\mathbf{r}_1, t_1) \psi_{\mathcal{U}}(\mathbf{r}_{1'}, t_{1'}) \rangle$, which is defined through the particle creation and destruction operators $\psi_{\mathcal{U}}^{(\dagger)}$ in the presence of an external, slowly varying disturbance $\mathcal{U}(\mathbf{r}, t)$. Namely,

$$f(\mathbf{p}, \mathbf{r}, t) = \int d\mathbf{x} \exp(-i\mathbf{p} \cdot \mathbf{x}) \langle \psi_{\mathcal{U}}^{\dagger}(\mathbf{r} + \mathbf{x}/2, 0) \psi_{\mathcal{U}}(\mathbf{r} - \mathbf{x}/2, t) \rangle, \tag{1}$$

where we have set $\hbar = 1$ and $\mathbf{r} = (\mathbf{r}_1 + \mathbf{r}_{1'})/2$ and $\mathbf{x} = \mathbf{r}_1 - \mathbf{r}_{1'}$ are the center of mass and the relative coordinate of the two particles. The moments of the Wigner function yield observables such as the particle density $n(\mathbf{r}, t) = (2\pi)^{-3} \int d\mathbf{p} f(\mathbf{p}, \mathbf{r}, t)$ and the current density $\mathbf{j}(\mathbf{r}, t) = (2\pi)^{-3} \int d\mathbf{p}(\mathbf{p}/m) f(\mathbf{p}, \mathbf{r}, t)$.

Contact with the Boltzmann transport equation is made by performing gradient expansions. As in the conventional Boltzmann-equation approach, the validity of the KB formulation is limited to slowly varying perturbations. On the other hand, the advantage of the KB formulation is that higher order correlations enter the equation of motion for the density matrix in an explicit manner, and therefore systematically improved approximations which are consistent with the conservation laws are accessible. Examples of such treatments of the correlation term are the Hartree–Fock approximation and the Born-collision approximation. In the former case the collisionless Boltzmann equation is recovered, while in the latter the collisional Boltzmann equation is extended to nondilute systems by including the effect of the external potential on the motion of the particles between collisions.

B. *Extension to Coupled Condensate–Noncondensate Dynamics*

The extension of the KB treatment to gases including a Bose-condensed component has been made by Kane and Kadanoff [19] and further developed by Griffin and co-workers [20, 22] and also by Wachter *et al.* [23] through a different derivation. The presence of two components and the appearence of off-diagonal elements in the density matrix (the so-called anomalous densities) below the Bose–Einstein condensation temperature requires the introduction of three Wigner distribution functions: $f_c(\mathbf{p}, \mathbf{r}, t)$ for the condensate component described by $\langle \psi_{\mathcal{U}}^{(\dagger)} \rangle$ and involving $|\langle \psi_{\mathcal{U}}^{\dagger} \rangle|^2$, $f_b(\mathbf{p}, \mathbf{r}, t)$ for the noncondensate described by the fluctuations operators $\tilde{\psi}_{\mathcal{U}}^{(\dagger)} \equiv \psi_{\mathcal{U}}^{(\dagger)} - \langle \psi_{\mathcal{U}}^{(\dagger)} \rangle$, and involving $\langle \tilde{\psi}_{\mathcal{U}}^{\dagger} \tilde{\psi}_{\mathcal{U}} \rangle$, and $f_m(\mathbf{p}, \mathbf{r}, t)$ for the anomalous part involving $\langle \tilde{\psi}_{\mathcal{U}} \tilde{\psi}_{\mathcal{U}} \rangle$ and its Hermitean conjugate.

We thus have to deal with the density of condensate $n_c(\mathbf{r}, t) = (2\pi)^{-3} \int d\mathbf{p} f_c(\mathbf{p}, \mathbf{r}, t)$, the density of noncondensate $n_b(\mathbf{r}, t) = (2\pi)^{-3} \int d\mathbf{p} f_b(\mathbf{p}, \mathbf{r}, t)$, and the anomalous density $m(\mathbf{r}, t) = (2\pi)^{-3} \int d\mathbf{p} f_m(\mathbf{p}, \mathbf{r}, t)$. Analogous expressions hold for the current densities.

As to the consistency of the approximations with the conservation laws, the same general remarks as for normal systems apply. However, the appearance of the condensate introduces an additional principle of gauge invariance, leading to the requirement that the excitation spectrum be gapless [26]. It is well known [20, 26] that approximations capable of simultaneously accommodating the conservation laws and the gaplessness condition are hardly available, so that a choice has to be made depending on the specific conditions of density and temperature of the system.

In the regime that we address in the present work the anomalous densities can be neglected, resulting in the gapless Hartree approximation [20, 23]. Thus, the equation of motion for the condensate wavefunction $\Phi(\mathbf{r}, t) \equiv \langle \psi_{\mathcal{U}}^{\dagger}(\mathbf{r}, t) \rangle$ is [21]

$$i\hbar \frac{\partial \Phi(\mathbf{r}, t)}{\partial t} = \left[-\frac{\hbar^2}{2m} \nabla^2 + V_{\mathrm{c,b}}^{\mathrm{eff}}(\mathbf{r}, t) \right] \Phi(\mathbf{r}, t) \tag{2}$$

and is coupled to the collisionless Vlasov equation for the noncondensate Wigner function $f_{\mathrm{b}}(\mathbf{p}, \mathbf{r}, t)$,

$$\frac{\partial f_{\mathrm{b}}(\mathbf{p}, \mathbf{r}, t)}{\partial t} + \frac{\mathbf{p}}{m} \cdot \nabla_{\mathbf{r}} f_{\mathrm{b}}(\mathbf{p}, \mathbf{r}, t) - \nabla_{\mathbf{r}} V_{\mathrm{b}}^{\mathrm{eff}}(\mathbf{r}, t) \cdot \nabla_{\mathbf{p}} f_{\mathrm{b}}(\mathbf{p}, \mathbf{r}, t) = 0. \tag{3}$$

The mean-field potentials in Eqs. (2) and (3) are

$$V_{\mathrm{c,b}}^{\mathrm{eff}}(\mathbf{r}, t) = V_{\mathrm{b}}^{\mathrm{ext}}(\mathbf{r}) + \mathcal{U}(\mathbf{r}, t) + U_{\mathrm{g}}[n_{\mathrm{c}}(\mathbf{r}, t) + 2n_{\mathrm{b}}(\mathbf{r}, t)] \tag{4}$$

and

$$V_{\mathrm{b}}^{\mathrm{eff}}(\mathbf{r}, t) = V_{\mathrm{b}}^{\mathrm{eff}}(\mathbf{r}) + \mathcal{U}(\mathbf{r}, t) + 2U_{\mathrm{g}}[n_{\mathrm{c}}(\mathbf{r}, t) + n_{\mathrm{b}}(\mathbf{r}, t)], \tag{5}$$

including the time-dependent driving potential $\mathcal{U}(\mathbf{r}, t)$ and an axially symmetric confining potential given for a harmonic trap by $V_{\mathrm{b}}^{\mathrm{eff}}(\mathbf{r}) = m_{\mathrm{b}}\omega_{\mathrm{b}}^2(r_{\perp}^2 + \epsilon_{\mathrm{b}}^2 z^2)/2$. In Eqs. (4) and (5), $n_{\mathrm{c}}(\mathbf{r}, t) = |\Phi(\mathbf{r}, t)|^2$ and $U_{\mathrm{g}} = 4\pi\hbar^2 a_{\mathrm{bb}}/m_{\mathrm{b}}$ is the boson–boson interaction parameter in terms of the s-wave scattering length a_{bb} and the boson mass m_{b}.

Once the algorithm to solve Eqs. (2) and (3) is implemented, it is easily extended to a mixture of condensed bosons and a fermionic cloud in the collisionless regime. In this case, the effective mean-field potentials become

$$V_{\mathrm{c,f}}^{\mathrm{eff}}(\mathbf{r}, t) = V_{\mathrm{b}}^{\mathrm{ext}}(\mathbf{r}) + \mathcal{U}(\mathbf{r}, t) + U_{\mathrm{g}}n_{\mathrm{c}}(\mathbf{r}, t) + U_{\mathrm{f}}n_{\mathrm{f}}(\mathbf{r}, t) \tag{6}$$

and

$$V_{\mathrm{f}}^{\mathrm{eff}}(\mathbf{r}, t) = V_{\mathrm{f}}^{\mathrm{ext}}(\mathbf{r}) + \mathcal{U}_{\mathrm{f}}(\mathbf{r}, t) + U_{\mathrm{f}}n_{\mathrm{c}}(\mathbf{r}, t). \tag{7}$$

Here, $V_{\mathrm{f}}^{\mathrm{ext}}(\mathbf{r}) = m_{\mathrm{f}}\omega_{\mathrm{f}}^2(r_{\perp}^2 + \epsilon_{\mathrm{f}}^2 z^2)/2$ and $\mathcal{U}_{\mathrm{f}}(\mathbf{r}, t)$ are the external trapping and driving potentials acting on the fermions and $U_{\mathrm{f}} = 2\pi\hbar^2 a_{\mathrm{bf}}/m_{\mathrm{r}}$ is the boson–fermion coupling constant with a_{bf} the boson–fermion s-wave scattering length and $m_{\mathrm{r}} = m_{\mathrm{b}}m_{\mathrm{f}}/(m_{\mathrm{b}} + m_{\mathrm{f}})$, where m_{f} is the fermion atomic mass. Notice that fermion–fermion interactions in the s-wave channel are effectively suppressed by the Pauli principle in a dilute gas of spin-polarized fermions, as is relevant to current experiments on boson–fermion mixtures.

C. *Validity of the Model*

To summarize, Eqs. (2) and (3) describe the coupled dynamics of a Bose–Einstein condensate and a bosonic or fermionic cold-atom cloud. In the former case the potentials $V_{c,b}^{eff}$ and V_b^{eff} are used, and in the latter these are replaced by $V_{c,f}^{eff}$ and V_f^{eff}. The range of validity of this approach is in principle limited to: (i) slowly varying space- and time-dependent external potentials, which allow a low-order gradient expansion of the equations of motion for the one-body density matrix; (ii) a collisionless regime, which allows expansion of the self-energies to first order in the strength of the atomic interactions; and (iii) not too low a temperature, so that the anomalous averages can be neglected and the Hartree–Fock spectrum is accurate.

We implement in the following a numerical method to solve Eqs. (2) and (3) and test it against dynamical behaviors in a one-component fermionic cloud and in clouds of either fermions or thermal bosons accompanied by a condensate. Of course, the role of the statistics enters at this level only from the initial distribution of the particles in phase space. We thus turn next to a discussion of the equations that we use to determine the initial conditions for the subsequent time evolution.

D. *Semiclassical Description of the Equilibrium State*

Before proceeding to present the algorithm for our dynamical simulations we briefly recall the basic steps that we take in preparing the initial state of the gas in thermodynamic equilibrium and in evaluating the corresponding densities of the condensate and of the fermionic or bosonic cloud. We refer the reader to Refs. [27, 28] for the details of the theory and for a discussion of the excellent agreement that it yields with thermodynamic data on Bose–Einstein condensed gases, under conditions of temperature and dilution that will be verified in the calculations reported in Section IV.

The equilibrium condensate density is calculated within the Thomas–Fermi approximation, which amounts to neglecting the kinetic energy term in the GPE. Its validity is ensured whenever the average mean-field energy $U_g n_c$ is much larger than the typical confining energy. In the case of harmonic confinement the condition $N_c a_{bb}/a_{ho} \gg 1$ is required, where N_c is the number of atoms in the condensate, $a_{ho} = (\hbar/m_b \bar{\omega}_b)^{1/2}$ is the harmonic oscillator length, and $\bar{\omega}_b = \omega_b \epsilon^{1/3}$ is the geometric average of the trap frequencies. The equilibrium density profile of the condensate is given by

$$n_c(\mathbf{r}) = \frac{1}{U_g}\left[\mu_b - V_b^{ext}(\mathbf{r}) - k_{b,f} n_{b,f}(\mathbf{r})\right]\theta\left(\mu_b - V_b^{ext}(\mathbf{r}) - k_{b,f} n_{b,f}(\mathbf{r})\right), \qquad (8)$$

where $k_b = 2U_g$, $k_f = U_f$, and μ_b is the chemical potential for the bosons.

For the equilibrium cloud density of bosons or fermions we adopt the semiclassical Hartree–Fock scheme [27]. This choice is justified as long as the gas is in a very dilute regime, a condition which is usually met in current experiments. In this approximation we have

$$n_{b,f}(\mathbf{r}) = \int \frac{d\mathbf{p}}{(2\pi)^3}\left\{\exp\left[\frac{1}{k_B T}\left(\frac{p^2}{2m_{b,f}} + V_{b,f}^{eff}(\mathbf{r}) - \mu_{b,f}\right)\right] \mp 1\right\}^{-1}, \qquad (9)$$

with $V_b^{eff}(\mathbf{r})$ and $V_f^{eff}(\mathbf{r})$ determined by the confining potentials supplemented by a static mean-field interaction term as in Eqs. (5) or (7).

The chemical potentials μ_b and μ_f are determined from the total numbers of bosons and fermions. In the case of a bosonic thermal cloud, μ_b is fixed by the relation

$$N_b = \int d\mathbf{r}[n_c(\mathbf{r}) + n_b(\mathbf{r})]. \tag{10}$$

For a fermionic cloud the chemical potential is determined from the total number of fermions,

$$N_f = \int d\mathbf{r}\, n_f(\mathbf{r}). \tag{11}$$

These equations complete the self-consistent closure of the model in the initial equilibrium state.

III. THE NUMERICAL METHOD

The set of Eqs. (2) and (3) for the condensate wavefunction and noncondensate Wigner function, respectively, bears a strong resemblance with self-consistent Vlasov–Poisson systems. The numerical study of Vlasov–Poisson equations was pioneered almost three decades ago in the context of plasma physics [29] and has ever since been the object of intense investigations using a variety of numerical techniques, including grid methods, particle methods, as well as hybrids thereof (see [30]). However, a systematic study of the applicability of these techniques to the physics of Bose–Einstein condensation is just beginning.

In this section we present details of the numerical procedure we have used to solve the system of Vlasov–Landau and Gross–Pitaevskii equations. Since most experimental setups are invariant under rotation in the azimuthal plane, we use cylindrical coordinates $\{r, z\}$. The wavefunction Φ is discretized on a two-dimensional grid of $N_r \times N_z$ points, which are uniformly distributed in a box of size $r_{max} \times 2z_{max}$: that is, $\Phi_{jk} \equiv \Phi(r_j, z_k)$ with

$$\begin{cases} r_j = (j-1)\Delta r & (j = 1, \ldots, N_r) \\ z_k = -z_{max} + (k-1)\Delta z & (k = 1, \ldots, N_z), \end{cases} \tag{12}$$

where Δr and Δz are the steps in the two space variables. The particle distributions are discretized by means of a set of P computational particles,

$$f(\mathbf{p}, \mathbf{r}, t) \rightarrow f_P(\mathbf{p}, \mathbf{r}, t) \equiv \sum_{i=1}^{P} \delta(\mathbf{r} - \mathbf{r}_i(t))\delta(\mathbf{p} - \mathbf{p}_i(t)), \tag{13}$$

where the $6P$ phase-space coordinates $\mathbf{r}_i(t)$ and $\mathbf{p}_i(t)$ represent the actual numerical unknowns entering the VLE. They obey Newton's equations,

$$\begin{cases} \frac{d\mathbf{r}_i}{dt} = \mathbf{p}_i/m \\ \frac{d\mathbf{p}_i}{dt} = \mathbf{F}_i, \end{cases} \tag{14}$$

where $\mathbf{F}_i$ collects all forces acting on the ith computational particle. As a result, at each time step we have to solve for $N_G = N_r N_z$ grid unknowns coupled to $6P$ discrete particle coordinates. To keep the systematic signal reasonably above the noise level, each grid cell contains of the order of 10–100 computational particles. As a result, $P \sim 10N_G - 100N_G$.

A. *Propagation of the Gross–Pitaevskii Equation*

The GPE is advanced in time by an explicit finite-difference method based on a nonstaggered variant of the Visscher method [31]. Full details are given in the original papers [10, 12] and here we shall just review the main ingredients of the algorithm. The basic idea is to advance the real and imaginary parts of the wavefunction, say A and B, in alternating steps,

$$\begin{cases} A_{jk}^{n+1} - A_{jk}^{n-1} = -2[K_{jk}(B) + V_{jk}^n(B)]\Delta t \\ B_{jk}^{n+1} - B_{jk}^{n-1} = 2[K_{jk}(A) + V_{jk}^n(A)]\Delta t, \end{cases} \tag{15}$$

where $n = 1, \ldots, N_T$ labels the discrete time sequence $t_n = n\Delta t$. The scheme is initiated as follows. The initial conditions specify the values of A and B at $n = 0$ and subsequently a first-order Euler step provides their values at $n = 1$. With these values available, all later steps $n = 2, 3, \ldots, N_T$ are taken by using Eqs. (15).

In Eqs. (15) K_{jk} is the kinetic energy operator,

$$K_{jk}(\Phi) = -\frac{\hbar^2}{2m}\left[\frac{\Phi_{j-1,k}}{\Delta r^2} + \frac{\Phi_{j+1,k}}{\Delta r^2} + \frac{\Phi_{j,k-1}}{\Delta z^2} + \frac{\Phi_{j,k+1}}{\Delta z^2} - 2\left(\frac{1}{\Delta r^2} + \frac{1}{\Delta z^2}\right)\Phi_{j,k}\right] \tag{16}$$

and

$$V_{jk}(\Phi) = V^{\text{eff}}(r_j, z_k; n_{jk})\Phi_{jk} \tag{17}$$

is the potential energy operator, which includes both external and self-consistent interaction terms. The self-consistent potential requires the specification of the particle density n_{jk} at each node of the spatial grid. This is obtained by convoluting the discrete particle distribution,

$$n_{jk}(t) = \sum_{i \in C_{jk}} W_{jk,i} f_i(t), \tag{18}$$

where C_{jk} is the grid cell centered at $r_{j+1/2} = (r_j + r_{j+1})/2$ and $z_{k+1/2} = (z_k + z_{k+1})/2$, while $f_i = 1$ if the particle belongs to C_{jk} and $f_i = 0$ otherwise. The factor $W_{jk,i}$ weights the contribution of particle i to the density at the grid point (r_j, z_k).

We adopt a bilinear cloud-in-cell (CIC) interpolator (see Fig. 1, top panel), which yields the scattering (particle-to-grid) rule [32]

$$W_{jk,i} = e_i(r_j)e_i(z_k) \quad (j = j_i, j_i + 1, \quad k = k_i, k_i + 1). \tag{19}$$

Here (j_i, k_i) identifies the lower left corner of the grid cell to which the ith particle belongs. In Eq. (19) $e_i(r)$ and $e_i(z)$ are one-dimensional piecewise linear splines centered on the discrete particle position (r_i, z_i),

$$e_i(r) = \begin{cases} 1 + \frac{(r-r_i)}{\Delta r} & (r_i - \Delta r < r < r_i) \\ 1 - \frac{(r-r_i)}{\Delta r} & (r_i < r < r_i + \Delta r), \end{cases} \tag{20}$$
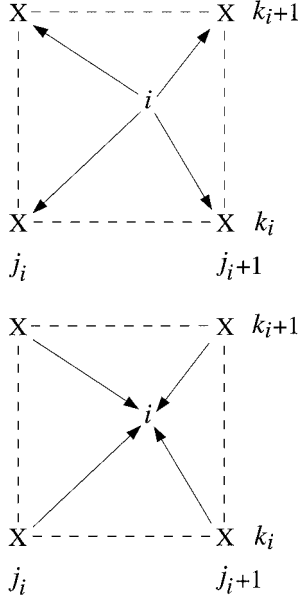
and similarly for $e_i(z)$.

FIG. 1. (Top) Bilinear CIC interpolation: contribution of particle i to the density at grid point (r_j, z_k). (Bottom) Bilinear CIC interpolation: contribution of the forces at grid point (r_j, z_k) to the force on particle i.

B. *Propagating the Vlasov–Landau Equation*

The VLE is advanced in time by a standard particle-in-cell (PIC) method [32]. In a modified Verlet time-marching scheme, we obtain the following set of discrete algebraic equations:

$$
\begin{cases}
r_i(t + \Delta t) = r_i(t) + v_{ri}(t)\Delta t + a_{ri}(t)\Delta t^2/2 \\
(r_i\theta_i)(t + \Delta t) = (r_i\theta_i)(t) + v_{\theta i}(t)\Delta t + a_{\theta i}(t)\Delta t^2/2 \\
z_i(t + \Delta t) = z_i(t) + v_{zi}(t)\Delta t + a_{zi}(t)\Delta t^2/2 \\
v_{ri}(t + \Delta t) = v_{ri}(t) + a_{ri}(t)\Delta t \\
v_{\theta i}(t + \Delta t) = v_{\theta i}(t) + a_{\theta i}(t)\Delta t \\
v_{zi}(t + \Delta t) = v_{zi}(t) + a_{zi}(t)\Delta t.
\end{cases}
\tag{21}
$$

Here a_r, a_θ, a_z and v_r, v_θ, v_z are the three components of the acceleration and velocity, respectively, along the (r, θ, z) coordinates. The advantage of the modified Verlet time marching is that it preserves fourth-order accuracy while synchronously keeping the coordinate and momentum degrees of freedom on the same sequence of discrete times.

The algorithm is standard except for the specification of the self-consistent coupling, namely, the force due to the density gradients. First, we form density gradients from auxiliary values of the density field $n_{j+1/2,k+1/2}$ at cell centers,

$$
\begin{cases}
Gr_{jk} = \left[n_{j+1/2,k-1/2} - n_{j-1/2,k-1/2} + n_{j+1/2,k+1/2} - n_{j-1/2,k+1/2} \right]/(2\Delta r) \\
Gz_{jk} = \left[n_{j-1/2,k+1/2} - n_{j-1/2,k-1/2} + n_{j+1/2,k+1/2} - n_{j+1/2,k-1/2} \right]/(2\Delta z).
\end{cases}
\tag{22}
$$

The azimuthal acceleration is zero in cylindrical symmetry. Next, the grid forces are

evaluated on the discrete particle locations, this being the inverse of the scattering operation discussed in the previous section (see Fig. 1, bottom panel). The grid-to-particle convolution is

$$\mathbf{F}_i = \sum_{s=0}^{1} W_{i,(j_i+s,k_i+s)} \mathbf{F}_{j_i+s,k_i+s}. \tag{23}$$

To avoid spurious self-forces we again use CIC interpolation, which amounts to using the same weighting function as for the GPE in the grid-to-particle scattering rule,

$$W_{i,jk} = e_j(r_i) e_k(z_i). \tag{24}$$

With the force/acceleration field transferred to the particle locations, everything is set to march the VLE in time.

C. *Boundary Conditions*

The conditions imposed on the wavefunction are (i) periodicity along the z coordinate, (ii) symmetry (zero radial gradient) at $r = 0$, and (iii) a vanishing value at the outer radial boundary $r = R$. For the discrete particle distribution we have again periodicity along z and specular reflection at the outer radial boundary. Specular reflection means that a particle flying from, say, $r_\alpha < R$ to $r_\beta > R$ is replaced by a particle at $r = 2R - r_\beta$ with inverted radial speed. Since the particle trajectories are tracked in a three-dimensional cylindrical coordinate frame, the $r = 0$ axis requires no special treatment.

1. Time-step considerations. The GPE and the VLE are advanced on the same discrete time sequence. This maximizes simplicity but implies that the time step is controlled by the fastest process at work, which usually is the self-consistent potential acting upon the condensate wavefunction. Better efficiency can be achieved by *subcycling* the time-stepper, namely, by advancing the slowest equation (say the VLE) only every $\Delta t_{VL}/\Delta t_{GP}$ steps, with Δt_{VL} and Δt_{GP} being the largest time steps allowed by the stability conditions on the two equations. The maximum time step for the GPE solver is estimated from

$$\Delta t_{GP} \left(C_1 \frac{\hbar}{m\delta^2} + C_2 \frac{V_M}{\hbar} \right) < 1, \tag{25}$$

where δ is a typical mesh size, V_M is the maximum value of the potential, and C_1 and C_2 are two $O(1)$ coefficients which depend on geometry and dimensionality. We note here the concurrent effects of quantum diffusion (kinetic energy) and scattering/absorption (potential energy).

The maximum time step for the VLE solver is estimated from

$$\Delta t_{VL} \frac{v_{max}}{\delta} < 1, \tag{26}$$

where v_{max} is the maximum speed in the velocity grid, which is of the order of the Fermi velocity for fermions and of the thermal velocity for bosons. Under ordinary conditions the kinetic energy contributions dominate over those from the potential energy, so that the condition for the GPE to be the time-limiting section of the code takes the form of a numerical "uncertainty principle," $mv_{max}\delta > \hbar$. For the cases discussed in this work, this

inequality is generally fulfilled within a factor of 10, so that subcycling is not compulsory. The inclusion of collisional interactions would make it mandatory.

2. Radial singularity. A source of potential trouble is the singularity at $r = 0$, which is known to affect all calculations in polar coordinates. To date, singular factors $1/r$ are regularized by a simple numerical cutoff $1/r \rightarrow 1/(r + r_c)$ with $r_c \sim 0.001\Delta r$, with a check that the physical results are virtually insensitive to the specific value of r_c.

Another undesirable side effect of the cylindrical geometry is the relative depletion of near-axis cells, which tend to host fewer particles just because of the $r\Delta r$ volumetric effect. On the other hand, this volumetric depletion is often more than compensated for by the physical behavior of the radial density, which is generally largest at $r = 0$. In any case, the volumetric effect can be readily disposed of by moving to a nonuniform grid along the radial coordinate.

3. Statistical noise. Considerations of statistical accuracy require of the order of a few tens of particles per grid point (or equivalently per grid cell) to keep the noise-to-signal ratio below an acceptable threshold. A practical consequence of this statistical accuracy requirement is that the VLE part of the computational scheme should be designed in such a way as to evolve these tens of computational particles in approximately the same amount of CPU time that it takes the GPE solver to advance a single grid point.

Another interesting consequence is that—at variance with ordinary situations in (classical) rarefied-gas dynamics—the number of computational particles in the simulation of Bose–Einstein condensates far exceeds the number of physical atoms, typically by a factor 10^3 in our case. As a result, each single computer simulation performs *de facto* a built-in ensemble average over a set of about a thousand realizations.

D. Procedure: Preparing the Initial State

The initial condition for the populations of bosons or fermions in the cold-atom cloud is prepared as follows. Particles are sampled from the probability distribution functions (pdf)

$$f_{b,f} = \frac{e^{-\eta}}{1 \mp e^{-\eta}}, \tag{27}$$

where $\eta \equiv \beta(p^2/2m + V_{\text{eff}} - \mu_{b,f})$ and $\beta = 1/k_B T$ is the inverse temperature.

The initializiation procedure starts by assigning to each spatial cell centered about position **r** a corresponding amount of computational particles,

$$\Delta N(\mathbf{r}) = n_{b,f}(\mathbf{r})\Delta V(\mathbf{r}), \tag{28}$$

where $\Delta V(\mathbf{r}) = 2\pi r \Delta r \Delta z$ is the cell volume. These particles must be sampled in momentum space according to the pdf (27). Owing to the nonseparability of the pdf, straightforward sampling based on exact inversion is ruled out and one must resort to more general—but less efficient—accept/reject methods.

The particle momenta are sampled from the distribution function using the standard Box–Mueller algorithm in three dimensions for cylindrical coordinates [33],

$$\begin{cases} p_\perp = p_{\text{max}} r_1 \\ \xi = 2\pi r_2 \\ p_z = p_{\text{max}}(2r_3 - 1), \end{cases} \tag{29}$$

where $r_1, r_2,$ and r_3 are sampled from a uniform distribution in the range $[0, 1]$. The maximum momentum p_{max} is taken to be of order $2p_F$ for cold fermions and of order $3m_b v_{th}$ for bosons, with $p_F = \hbar k_f$ being the Fermi momentum and v_{th} being the average thermal velocity. The particle momentum coordinates in the azimuthal plane are evaluated as

$$\begin{cases} p_r = p_\perp \sin\xi \\ p_\theta = p_\perp \cos\xi. \end{cases} \tag{30}$$

Finally, to avoid poor acceptance rates, the standard accept/reject test is performed by comparing the pdf with the maximum value $f_{max}(\mathbf{r})$ that it can take in the cell at position $\mathbf{r}$, that is,

$$If\ f(p_r, p_\theta, p_z; \mathbf{r}) > r_4 f_{max}(\mathbf{r}) : accept$$
$$Else : reject, \tag{31}$$

where r_4 is a random number uniformly distributed in $[0, 1]$.

IV. PHYSICAL APPLICATIONS

A. *Expansion of Cold Fermions*

As a first test of the dynamical algorithm, we consider the expansion of a cloud of cold fermions after release of the harmonic trap. The neglect of the collisional integrals is a reliable approximation in this context, since, as already remarked, the s-wave scattering between spin-polarized fermions is suppressed by the Pauli principle.

This problem has been analytically solved in Ref. [34] under the assumption of ballistic expansion. The time evolution of the mean square radii is found to be

$$\langle r_\perp^2(t) \rangle = \frac{1}{3N_f} E_{rel} \frac{4}{m_f \omega_f^2} \left(1 + \omega_f^2 t^2\right) \tag{32}$$

and

$$\langle z^2(t) \rangle = \frac{1}{3N_f} E_{rel} \frac{2}{m_f(\epsilon_f \omega_f)^2} (1 + (\epsilon_f \omega_f)^2 t^2). \tag{33}$$

In Eqs. (32) and (33) E_{rel} is the so-called release energy, namely, the energy of the system with N_f fermions after switching off the trap, which amounts to one half of the total average energy. For a noninteracting fermion gas at temperature $T > 0.2T_F$ this is best approximated by the classical relation $E_{rel} \simeq 3N_f k_B T/2$, while at lower temperature it is given by $E_{rel} \simeq (3/4)N_f E_F[1 + (2\pi/3)(T/T_F)^2]$, with $E_F = k_B T_F = (6N_f)^{1/3}\hbar\omega_f$ being the Fermi energy.

We prepare the initial thermodynamic state (9) for $N_f = 1000$ ^{40}K atoms in an isotropic trap with $\omega_f = 2\pi \times 15.92$ rad/s at $T = 0.55T_F \approx 7.6$ nK. The chemical potential of the gas is $\mu_f = 0.063E_F = 1.14\hbar\omega_f$. We use an $N_r \times N_z$ Mesh of 201×401 points with 1.6×10^6 representative particles in a box measuring 40 and 80 in units of $a_{ho} = \sqrt{\hbar/(m_f\omega_f)}$ along the radial and axial directions, respectively. The time step in the dynamical simulation is $\omega_f \Delta t = 10^{-4}$.

We then evaluate from the simulation runs the radial width

$$\sigma_{r_\perp}(t) = \sqrt{\int dx\,dy\,dz[(x(t) - \langle x(t)\rangle)^2 + (y(t) - \langle y(t)\rangle)^2]n_{\mathrm{f}}(\mathbf{r}; t)}$$

$$= \frac{1}{P}\sum_{i=1}^{P}[(x_i(t) - \langle x(t)\rangle)^2 + (y_i(t) - \langle y(t)\rangle)^2] \tag{34}$$

and the axial width

$$\sigma_z(t) = \sqrt{\int dx\,dy\,dz(z(t) - \langle z(t)\rangle)^2 n_{\mathrm{f}}(\mathbf{r}; t)}$$

$$= \frac{1}{P}\sum_{i=1}^{P}(z_i(t) - \langle z(t)\rangle)^2 \tag{35}$$

of the cloud as functions of time, after averaging over the density distribution $n_{\mathrm{f}}(\mathbf{r}; t)$ by means of sum over all particles positions. Here, the center-of-mass coordinates are defined as $\langle x(t)\rangle = \sum_{i=1}^{P} x_i(t)/P$ and similarly for $\langle y(t)\rangle$ and $\langle z(t)\rangle$. Of course, during free expansion the center-of-mass coordinates must remain unchanged: This property is used as a test of the numerical method.

Figure 2 shows that the calculated $\sigma_{r_\perp}$ (circles) and σ_z (squares) agree with the results from the analytical expressions (32) and (33) (solid lines), where the classical expression has been used for E_{rel}. Snapshots of the density profiles at selected times are shown as contour plots in Fig. 3. The definition of the profile degrades in time because the number of particles per cell drops during the expansion.

After this test of the reliability of the simulation method, we proceed to use it in some original applications.
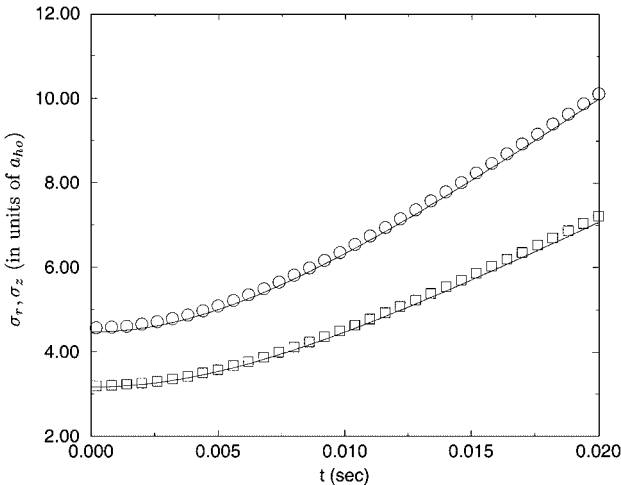

FIG. 2.   Expansion of a cold fermionic cloud after release from a harmonic trap: radial and axial widths of the density distribution (in units of a_{ho}) as functions of time. Circles, $\sigma_{r_\perp}$; squares, σ_z; solid lines, analytical expressions (32) and (33) from Ref. [34].
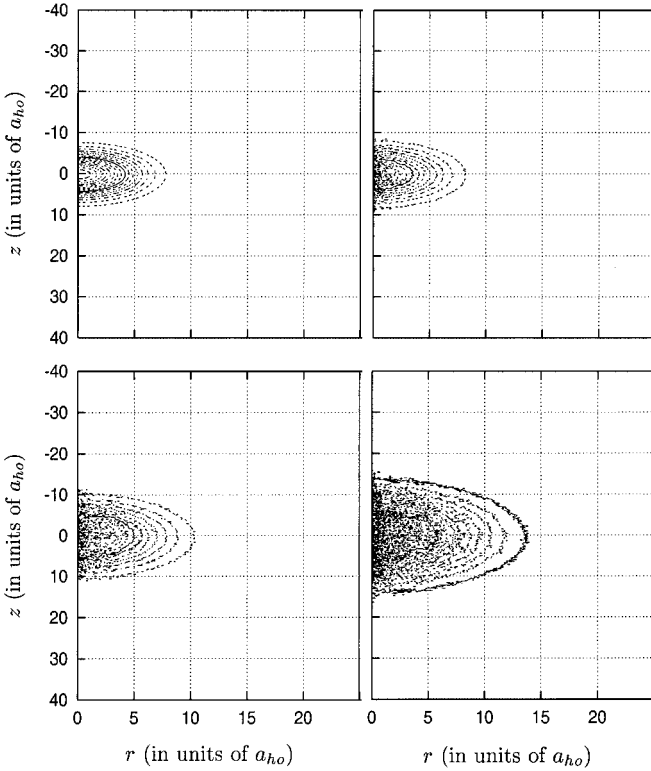
FIG. 3. Expansion of a cold fermionic cloud after release from a harmonic trap: snapshots of the density distribution, shown as contour plots. From top left to bottom right: $t = 0$, 5, 10, and 15 ms. The axial and radial coordinates are in units of a_{ho}.

B. *Expansion of a Mixture of a Condensate and a Cold-Fermion Cloud*

As a first novel application we look at the case in which a core of Bose-condensed atoms is present inside the dilute Fermi gas. We prepare a state with $N_f = 1000$ ^{40}K atoms and $N_c = 10^5$ ^{39}K atoms in identical harmonic traps and at the same temperature as for the Fermi gas studied in Section IV.A. The scattering length which describes the interactions between the atoms in the condensate is $a_{bb} = 80 a_{Bohr}$, while the interspecies scattering length is $a_{bf} = 40 a_{Bohr}$.

The inclusion of the GPE algorithm at fixed mesh size normally requires shorter time steps to mantain stability. We make the choice of a thinner 501×1001 mesh than that in Section IV.A to keep the time step at $\omega \Delta t = 10^{-4}$, with all other simulation parameters remaining the same.

The initial state is characterized by $\mu_b = 0.52 E_F = 9.51 \hbar \omega_f$ and $\mu_f = 0.10 E_F = 1.83 \hbar \omega_f$. We display in Fig. 4 the average widths $\sigma_{r_\perp}$ (circles) and σ_z (squares) for both the fermionic cloud (open symbols) and the condensate (filled symbols). The solid lines are the analytical solution for the ideal Fermi cloud as in Fig. 2. It is seen that with the scattering lengths of the ^{39}K–^{40}K mixture the mean-field force of the inner condensate core on the outer fermionic cloud is not strong enough to sizeably affect the expansion of the latter.

Snapshots of the condensate density profiles and of the fermionic cloud at times $t = 0$, 8.5, 17, and 25.5 ms are displayed as contour plots in Figs. 5 and 6. Comparison with
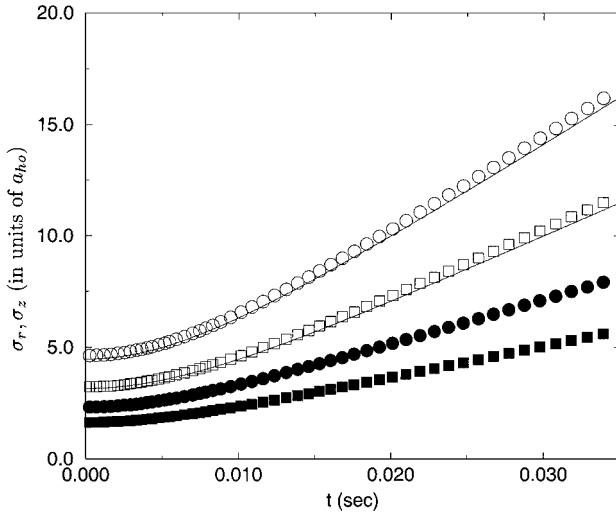
FIG. 4. Expansion of a cold fermionic cloud and an inner condensate core after release from a harmonic trap: radial and axial widths of the density distributions (in units of a_{ho}) as functions of time. Circles, $\sigma_{r_\perp}$; squares, σ_z; open symbols, fermionic cloud; filled symbols, condensate; solid lines, analytical expressions (32) and (33) from Ref. [34].
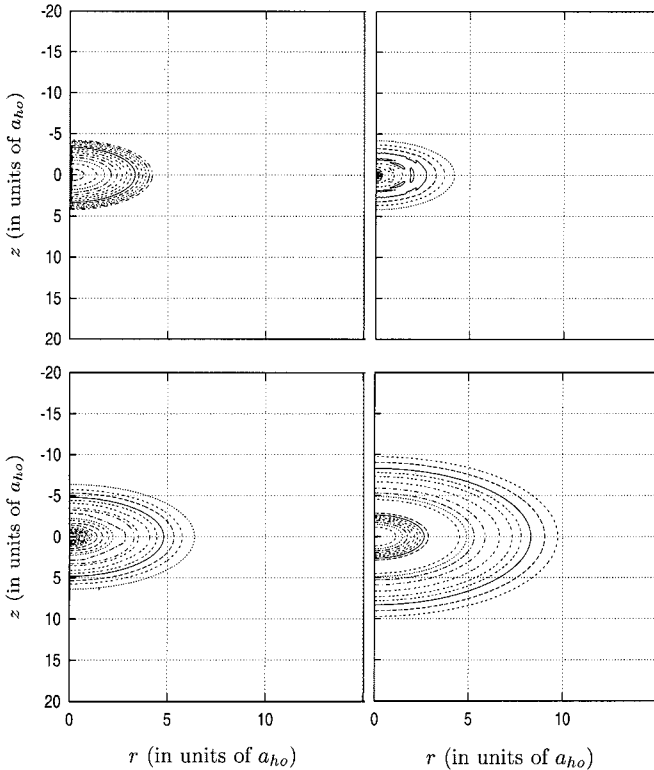

FIG. 5. Expansion of a cold fermionic cloud with an inner condensate core after release from a harmonic trap: snapshots of the condensate density distribution, shown as contour plots. From top left to bottom right: $t = 0$, 8.5, 17, and 25.5 ms. The axial and radial coordinates are in units of a_{ho}.
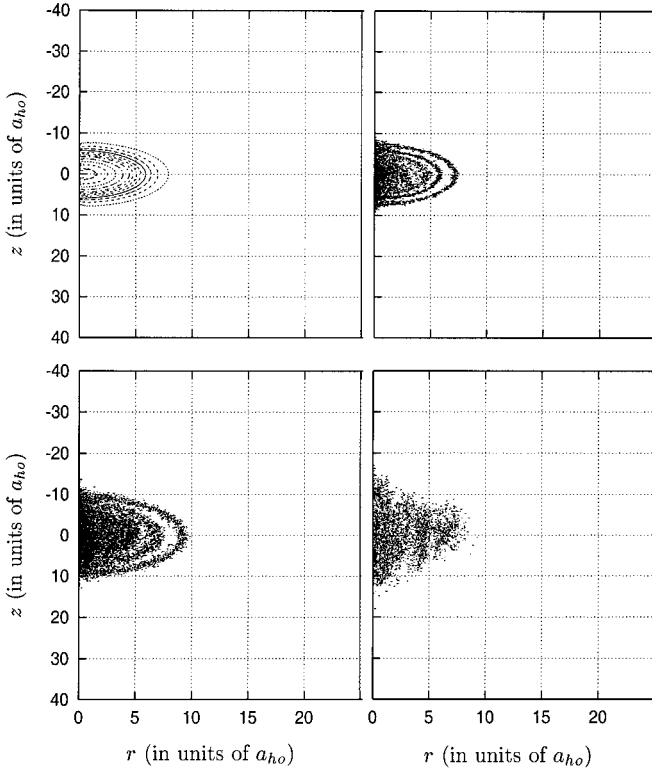
FIG. 6. Expansion of a cold fermionic cloud with an inner condensate core after release from a harmonic trap: snapshots of the fermionic density distribution, shown as contour plots. From top left to bottom right: $t = 0$, 8.5, 17, and 25.5 ms. The axial and radial coordinates are in units of a_{ho}.

those in Fig. 3 shows that the reduced number of computational particles per cell tends to increase the statistical noise. This degradation worsens as the simulational time elapses, as is evidenced by the last snapshot in Fig. 6.

C. *Oscillations of Bose Gases inside an Optical Lattice*

Here and in the following section we apply our numerical method to study the dynamics of a Bose–Einstein condensate and a thermal cloud of ^{87}Rb atoms at finite temperature inside a one-dimensional optical lattice. The initial state is prepared by adding to the harmonic trap, described by $V_{\text{trap}}(\mathbf{r}) = (1/2)m\omega^2(r_\perp^2 + \epsilon^2 z^2)$, a periodic potential given by $V_{\text{latt}}(z) = \alpha E_R \sin^2(k_L z)$, where $E_R = \hbar^2 k_L^2/(2m)$ is the recoil energy and $k_L = 2\pi/\lambda$ is the wavenumber of the laser beam which creates an optical lattice with period π/k_L in the axial direction.

Such a system, which has been realized at LENS [35] and examined numerically at $T = 0$ by two of us [35, 36], shows a rich variety of dynamical behaviors. Thus, the study of the sloshing-mode oscillations of an almost pure condensate with $N = 3 \times 10^5$ atoms in a lattice with $\alpha = 1.6$ shows that superfluidity is superseded by dissipation as the initial displacement of the condensate away from the harmonic-trap center is increased. This behavior is quantitatively understood as a gradual destruction of superfluidity via emission of sound waves in the periodically modulated inhomogeneous medium [35]. Below the
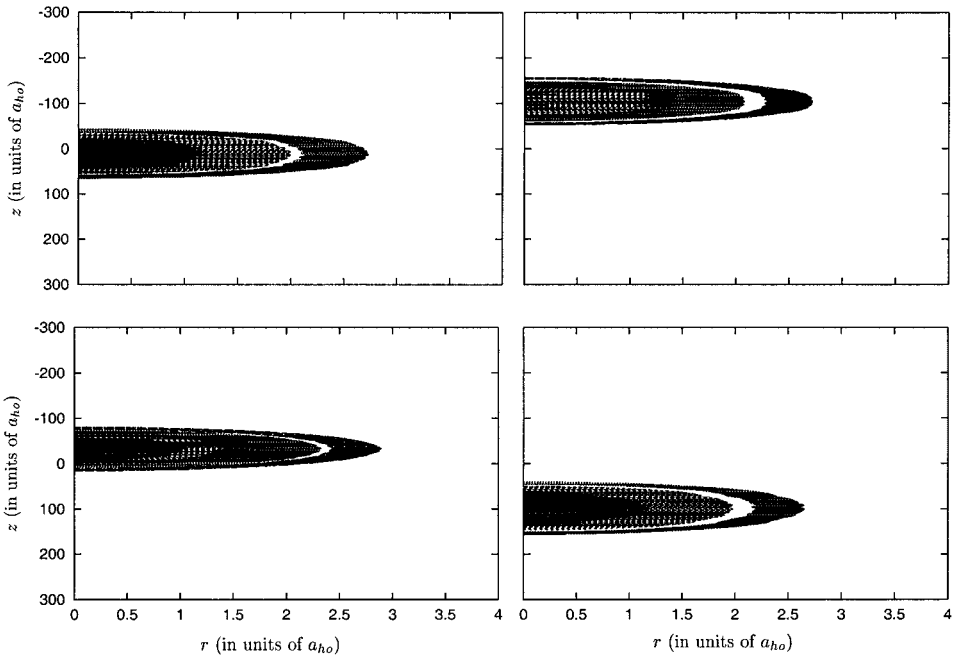
FIG. 7. Oscillations of a condensate in a harmonic plus shallow optical-lattice potential: snapshots of the density distribution, shown as contour plots. From top left to bottom right: $t = 23.3, 46.6, 69.9$, and 93.2 ms. The axial and radial coordinates are in units of a_{ho}.

dissipative threshold, on the other hand, the oscillatory motion of the condensate through the optical lattice can be mapped into the dynamics of superconducting carriers through a weak-link Josephson junction [36]. This implies the possibility of observable resonances and of multimode behavior.

Here we extend our numerical studies to contrast the oscillations of a condensate with the motions of a thermal cloud. We prepare initial states for the two cases $\alpha = 1$ and $\alpha = 5$, both at $T = 0$ for the BEC [37] and for the thermal cloud at temperature T above the critical temperature T_c. We give an initial displacement $\Delta z = 42.6\ \mu$m to the trap center and follow the subsequent dynamics with a time step $\omega \Delta t$ of order 10^{-5}.

The snapshots of the atomic density show that for $\alpha = 1$ (see Figs. 7 and 8) the condensate behaves as a superfluid executing harmonic oscillations at a frequency equal to the trap frequency, while the thermal cloud at $T > T_c$ diffuses away in a quarter of a period. For $\alpha = 5$ (see Figs. 9 and 10) the condensate instead breaks into fragments as it attempts to perform the first oscillation, and after a period its center of mass becomes localized at the bottom of the harmonic well. In the same setup the thermal cloud becomes localized at the center of the trap in $1/10$ of a period and spreads out.

Figure 11 gives a clear picture of these behaviors by reporting the axial center position and width of the condensate and of the thermal cloud as functions of time in the two cases.

D. *Expansion of a Bose-Condensed Gas in an Optical Lattice*

In our final study we look at the expansion of a Bose–Einstein condensate and its thermal cloud, which initially reside in a harmonic well and a superposed optical-lattice
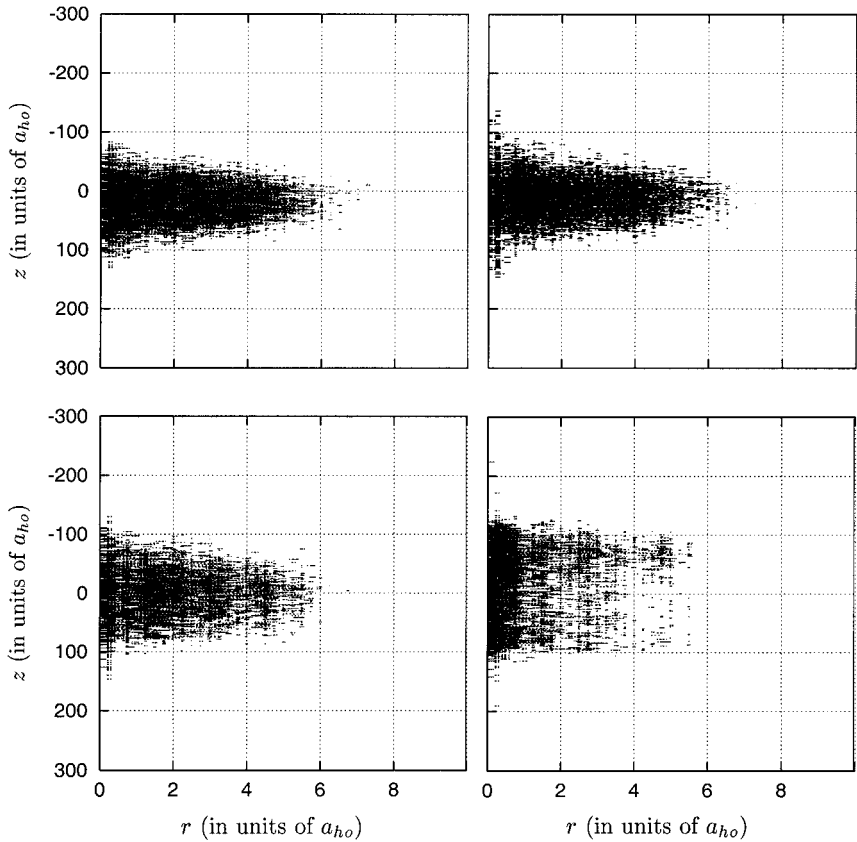
FIG. 8. Oscillations of a bosonic thermal cloud in a harmonic plus shallow optical-lattice potential: snapshots of the density distributions, shown as contour plots. From top left to bottom right: $t = 6$, 12, 18, and 24 ms. The axial and radial coordinates are in units of a_{ho}.

potential. The external potentials are characterized by parameters typical of an experiment at LENS [38], namely, $\omega = 2\pi \cdot 90$ rad/s, $\epsilon = 8.9/90$, $2\pi/k_L = 795$ nm, and $\alpha = 5$. The condensate contains 6935 ^{87}Rb atoms and the thermal cloud is composed of 3065 atoms. The temperature of the gas is $T = 86$ nK $= 0.24 E_R/k_B$ and its chemical potential is $\mu = 5.86\hbar\omega = 0.14 E_R$. We use a mesh of 111×2801 points with 308,000 representative particles.

We evolve the gas with a time step $\omega\Delta t = 7 \times 10^{-5}$ after switching off both the harmonic trap and the periodic potential. Snapshots of the atomic densities of the condensate and of its thermal cloud, taken at the moment in which the potentials are switched off and after 3.5, 7, and 10.5 ms of free expansion, are shown in Figs. 12 and 13. The condensate is seen in Fig. 12 to develop side bands which separate out of the central cloud, while the thermal cloud in Fig. 13 simply spreads out. These features of our numerical results reproduce those observed in the experiments [38].

The appearance of side bands in the condensate during expansion is due to Bragg scattering against the periodic potential. In fact, in a long-time simulation run of a one-dimensional model of the expansion we have found that the condensate side bands move at velocity $v \simeq 2\hbar k_L/m$, corresponding to the momentum associated with the first reciprocal vector of the optical lattice.
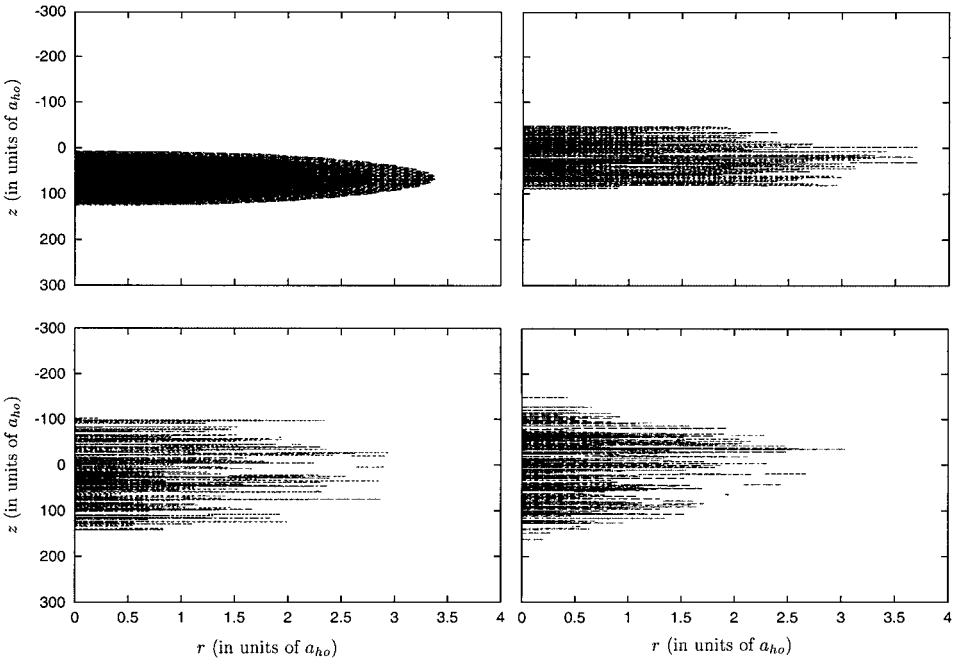
FIG. 9. Oscillations of a condensate in a harmonic plus deep optical-lattice potential: snapshots of the density distributions, shown as contour plots. From top left to bottom right: $t = 23.3$, 46.6, 69.9, and 93.2 ms. The axial and radial coordinates are in units of a_{ho}.

V. COMPUTATIONAL REMARKS

We have assessed the computational performance of the numerical method by repeating the test of Section IV.A after changing either the number of computational particles or the mesh size. We list in Table I the computational times elapsed while running the HPF-PGI-compiled code on a fully dedicated 1-GHz Pentium III SCSI.

These data provide the following values for the specific CPU time costs of the GPE and VLE of the code per time step:

$$\begin{cases} t_{GP} \sim 1.5 \, \mu s/\text{grid point} \\ t_{VL} \sim 0.6 \, \mu s/\text{particle}. \end{cases} \tag{36}$$

TABLE I
Expansion of a Cloud of Fermionic ^{40}K Atoms after
Release from the Harmonic Trap

P	$N_r \times N_z$	CPU time (hh:mm:ss)
1.6×10^6	201×401	8:35:27
8×10^5	201×401	5:33:55
1.6×10^6	401×801	10:22:24

Note. CPU time (third column) elapsed on a 1-GHz Pentium III SCSI for simulating 20,000 time steps, corresponding to 20 ms, for various numbers of computational particles (first column) and mesh sizes (second column).
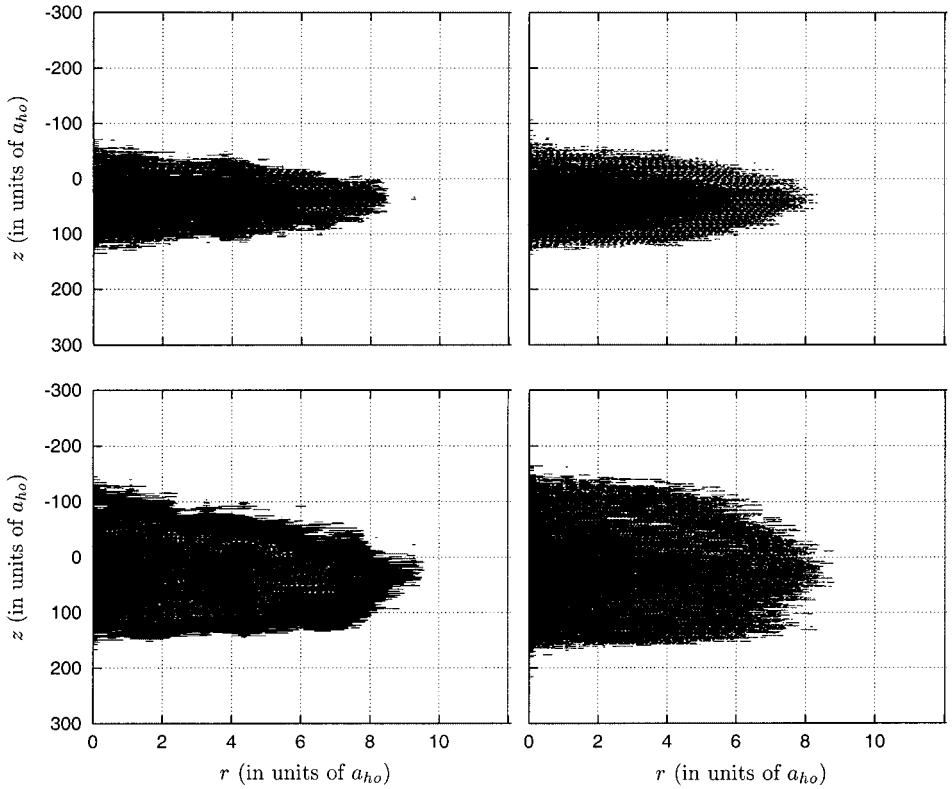
FIG. 10. Oscillations of a bosonic thermal cloud in a harmonic plus deep optical-lattice potential: snapshots of the density distributions, shown as contour plots. From top left to bottom right: $t = 2.8$, 5.6, 8.4, and 11.2 ms. The axial and radial coordinates are in units of a_{ho}.
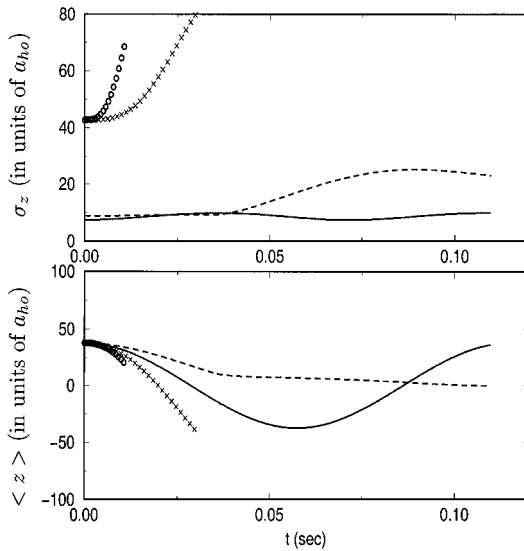

FIG. 11. Oscillations of a condensate and a bosonic thermal cloud in a harmonic trap plus optical-lattice potential with axial center-of-mass coordinate and average axial width of the density distributions (in units of a_{ho}) as functions of time. Continuous line, condensate with $\alpha = 1$; dashed line, condensate with $\alpha = 5$; crosses, thermal cloud with $\alpha = 1$; circles, thermal cloud with $\alpha = 5$.
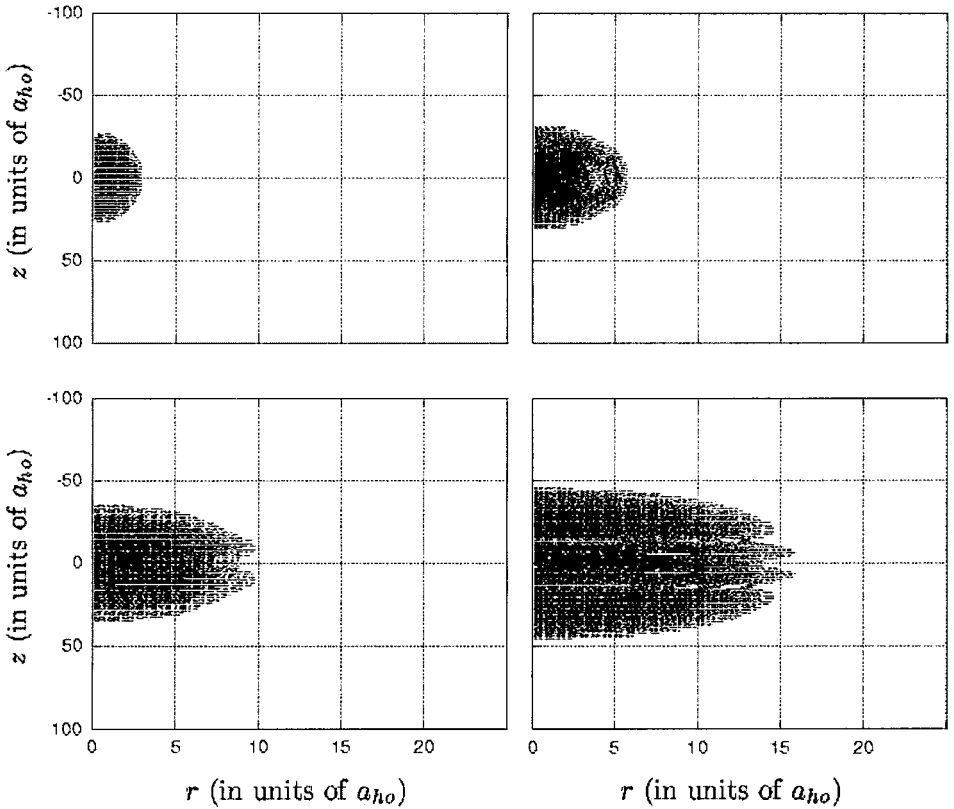
FIG. 12. Expansion of a condensate interacting with its thermal cloud after release from harmonic plus deep optical-lattice potential: snapshots of the density distribution, shown as contour plots. From top left to bottom right: $t = 0$, 3.5, 7, and 11.5 ms. The axial and radial coordinates are in units of a_{ho}.

These figures invite a number of comments. First, they show that the VLE section can evolve just a few computational particles while a single grid point of the GPE solver is advanced. This is not surprising on account of the explicit nature of the GPE solver. Since statistical accuracy requires of the order of 10 particles per cell, we conclude that the VLE solver is a potential computational bottleneck. Let us nonetheless assume that the VLE and GPE sections can evolve on a one-to-one CPU time basis. We can then focus on the grid part only and estimate the feasibility of large-scale applications to finite-temperature condensates in optical lattices. Covering a simulation span of 100 ms in steps of 0.1 μs requires 10^7 time steps. At a cost of 1 μs per time step and grid point, a grid with, say, 10^6 points takes of the order of 10^6 s—almost two weeks—of CPU time to complete. Ways to achieve substantial speed-up are clearly needed. Among others, a promising strategy is parallel computing, possibly combined with nonuniform meshes. The efficient implementation of such parallel schemes is a nontrivial task which requires a careful analysis [39]. The standing challenge is again associated with the Vlasov equation.

The parallelization of the GPE solver alone would proceed via a straightforward geometrical decomposition of the computational grid, whereby each processor would own the values of the condensate wavefunction at the grid points belonging to the given geometrical subdomain. Such a static geometric decomposition faces potential efficiency problems in the parallel Vlasov solver, simply because the set of particles owned by any given processor
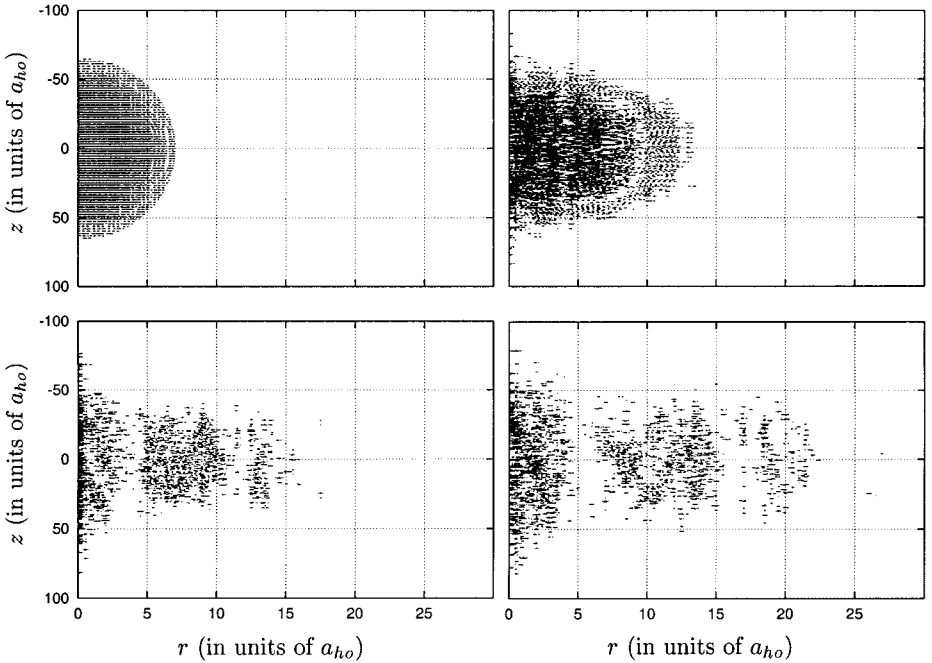
FIG. 13. Expansion of a bosonic thermal cloud interacting with a condensate after release from harmonic plus deep optical-lattice potential: snapshots of the density distribution, shown as contour plots. From top left to bottom right: $t = 0, 3.5, 7$, and 11.5 ms. The axial and radial coordinates are in units of a_{ho}.

is changing all the time due to particle motion. As a result, a substantial amount of interprocessor communication is required to keep this information up to date. One may of course partition over the set of particles, i.e., assign each processor with a static subset of particles regardless of their position in space. A complementary problem is immediately apparent, though: Particles interacting in the same mesh cell are now likely to belong to many different processors, whence again entailing the need of performance-degrading interprocessor communications. These simple considerations highlight the fact that the efficient implementation of parallel solvers for grid–particle methods requires a careful tradeoff, whose actual outcome may well depend on the architectural details of the parallel computer at hand. Fortunately, in the last decade much activity has been directed to this problem in the field of parallel computing. The optimal adaptation of this current know-how to the context of Bose–Einstein condensates is surely an important issue of future research in the field.

VI. CONCLUDING REMARKS

The increasing complexity and variety of phenomena observed in current studies of the dynamical behavior of normal and superfluid quantum gases at finite temperature motivate the development of suitable numerical tools to assist theoretical understanding.

To this aim, we have combined a particle-in-cell method with an explicit time-marching algorithm to evaluate the time evolution in models of a Bose–Einstein condensate and a cold-atom cloud.

We have tested the method against known analytical results in the simple physical situations offered by the expansion of a collisionless fermionic cloud without and with an

inner Bose-condensed core. We have also applied it to simulate novel experimental observations on the dynamical behavior of a condensate with its thermal cloud in a harmonic plus optical-lattice potential, where we have found substantial accord with current experiments.

We have also analyzed those computational aspects of the algorithm which are most relevant to applications in large-scale problems. This analysis emphasizes the need for nonuniform meshes and parallel computing. On the physics front, an extension of the method to include the quantum collisional integrals is underway.

ACKNOWLEDGMENTS

REFERENCES

1. M. H. Anderson, J. R. Ensher, M. R. Matthews, C. E. Wieman, and E. A. Cornell, Observation of Bose–Einstein condensation in a dilute atomic vapor, *Science* **269**, 198 (1995); K. B. Davis, M.-O. Mewes, M. R. Andrews, N. J. van Druten, D. S. Durfee, D. M. Kurn, and W. Ketterle, Bose–Einstein condensation in a gas of sodium atoms, *Phys. Rev. Lett.* **75**, 3969 (1995); C. C. Bradley, C. A. Sackett, and R. G. Hulet, Bose–Einstein condensation of lithium: Observation of limited condensate number, *Phys. Rev. Lett.* **78**, 985 (1997); D. G. Fried, T. C. Killian, L. Willmann, D. Landhuis, S. C. Moss, D. Kleppner, and T. J. Greytak, Bose–Einstein condensation of atomic hydrogen, *Phys. Rev. Lett.* **81**, 3811 (1998); F. Pereira Dos Santos, J. Léonard, J. Wang, C. J. Barrelet, F. Perales, E. Rasel, C. S. Unnikrishnan, M. Leduc, and C. Cohen-Tannoudji, Bose–Einstein condensation of metastable helium, *Phys. Rev. Lett.* **86**, 3459 (2001).

2. D. S. Jin, J. R. Ensher, M. R. Matthews, C. E. Wieman, and E. A. Cornell, Collective excitations of a Bose–Einstein condensate in a dilute gas, *Phys. Rev. Lett.* **77**, 420 (1996); M.-O. Mewes, M. R. Andrews, N. J. van Druten, D. M. Kurn, D. S. Durfee, C. G. Townsend, and W. Ketterle, Collective excitations of a Bose–Einstein condensate in a magnetic trap, *Phys. Rev. Lett.* **77**, 988 (1996); J. R. Ensher, D. S. Jin, M. R. Matthews, C. E. Wieman, and E. A. Cornell, Bose–Einstein condensation in a dilute gas: Measurement of energy and ground-state occupation, *Phys. Rev. Lett.* **77**, 4984 (1996); D. S. Jin, M. R. Matthews, J. R. Ensher, C. E. Wieman, and E. A. Cornell, Temperature-dependent damping and frequency shifts in collective excitations of a dilute Bose–Einstein condensate, *Phys. Rev. Lett.* **78**, 764 (1997); M. R. Andrews, D. M. Kurn, H.-J. Miesner, D. S. Durfee, C. G. Townsend, S. Inouye, and W. Ketterle, Propagation of sound in a Bose–Einstein condensate, *Phys. Rev. Lett.* **79**, 553 (1997); D. M. Stamper-Kurn, H.-J. Miesner, S. Inouye, M. R. Andrews, and W. Ketterle, Collisionless and hydrodynamic excitations of a Bose–Einstein condensate, *Phys. Rev. Lett.* **81**, 500 (1998); R. Onofrio, D. S. Durfee, C. Raman, M. Köhl, C. E. Kuklewicz, and W. Ketterle, Surface excitations of a Bose–Einstein condensate, *Phys. Rev. Lett.* **84**, 810 (2000).

3. M.-O. Mewes, M. R. Andrews, D. M. Kurn, D. S. Durfee, C. G. Townsend, and W. Ketterle, Output coupler for Bose–Einstein condensed atoms, *Phys. Rev. Lett.* **78**, 582 (1997); B. P. Anderson and M. Kasevich, Macroscopic quantum interference from atomic tunnel array, *Science* **282**, 1686 (1998); I. Bloch, T. W. Hänsch, and T. Esslinger, Atom laser with a cw output coupler, *Phys. Rev. Lett.* **82**, 3008 (1999); E. W. Hagley, L. Deng, M. Kozuma, J. Wen, K. Helmerson, S. L. Rolston, and W. D. Phillips, A well-collimated quasi-continuous atom laser, *Science* **283**, 1706 (1999); O. M. Maragò, S. A. Hopkins, J. Arlt, E. Hodby, G. Hechenblaikner, and C. J. Foot, Observation of the scissors mode and evidence for superfluidity of a trapped Bose–Einstein condensed gas, *Phys. Rev. Lett.* **84**, 2056 (2000); A. P. Chikkatur, A. Görlitz, D. M. Stamper-Kurn, S. Inouye, S. Gupta, and W. Ketterle, Suppression and enhancement of impurity scattering in a Bose–Einstein condensate, *Phys. Rev. Lett.* **85**, 483 (2000); R. Onofrio, C. Raman, J. M. Vogels, J. R. Abo-Shaeer, A. P. Chikkatur, and W. Ketterle, Observation of superfluid flow in a Bose–Einstein condensed gas *Phys. Rev. Lett.* **85**, 2228 (2000); O. M. Maragò, G. Hechenblaikner, E. Hodby, and C. J. Foot, Temperature dependence of damping and frequency shifts of the scissors mode of a trapped Bose–Einstein condensate, *Phys. Rev. Lett.* **86**, 3938 (2001).

4. S. Inouye, A. P. Chikkatur, D. M. Stamper-Kurn, J. Stenger, D. E. Pritchard, and W. Ketterle, Superradiant Rayleigh scattering from a Bose–Einstein condensate, *Science* **285**, 571 (1999); M. Kozuma, L. Deng, E. W. Hagley, J. Wen, R. Lutwak, K. Helmerson, S. L. Rolston, and W. D. Phillips, Coherent splitting of Bose–Einstein condensed atoms with optically induced Bragg diffraction, *Phys. Rev. Lett.* **82**, 871 (1999); J. Stenger, S. Inouye, A. P. Chikkatur, D. M. Stamper-Kurn, D. E. Pritchard, and W. Ketterle, Bragg spectroscopy of a Bose–Einstein condensate, *Phys. Rev. Lett.* **82**, 4569 (1999); M. Kozuma, Y. Suzuki, Y. Torii, T. Sugiura, T. Kuga, E. W. Hagley, and L. Deng, Phase-coherent amplification of matter waves, *Science* **286**, 2309 (1999); J. Denschlag, J. E. Simsarian, D. L. Feder, C. W. Clark, L. A. Collins, J. Cubizolles, L. Deng, E. W. Hagley, K. Helmerson, W. P. Reinhardt, S. L. Rolston, B. I. Schneider, and W. D. Phillips, Generating solitons by phase engineering of a Bose–Einstein condensate, *Science* **287**, 97 (2000).

5. M. R. Matthews, B. P. Anderson, P. C. Haljan, D. S. Hall, C. E. Wieman, and E. A. Cornell, Vortices in a Bose–Einstein condensate, *Phys. Rev. Lett.* **83**, 2498 (1999); K. W. Madison, F. Chevy, W. Wohlleben, and J. Dalibard, Vortex formation in a stirred Bose–Einstein condensate, *Phys. Rev. Lett.* **84**, 806 (2000); J. R. Abo-Shaeer, C. Raman, J. M. Vogels, and W. Ketterle, Observation of vortex lattices in Bose–Einstein condensates, *Science* **292**, 476 (2001).

6. B. DeMarco and D. S. Jin, Onset of Fermi degeneracy in a trapped atomic gas, *Science* **285**, 1703 (1999); B. DeMarco, S. B. Papp, and D. S. Jin, Pauli blocking of collisions in a quantum degenerate atomic Fermi gas, *Phys. Rev. Lett.* **86**, 5409 (2001); S. D. Gensemer and D. S. Jin, Transition from collisionless to hydrodynamic behavior in an ultracold Fermi gas, *Phys. Rev. Lett.* **87**, 173201 (2001); B. DeMarco and D. S. Jin, Spin excitations in a Fermi gas of atoms, cond-mat/0109098 (2001).

7. F. Schreck, L. Khaykovich, K. L. Corwin, G. Ferrari, T. Bourdel, J. Cubizolles, and C. Salomon, Quasipure Bose–Einstein condensate immersed in a Fermi sea, *Phys. Rev. Lett.* **87**, 080403 (2001); A. G. Truscott, K. E. Strecker, W. I. McAlexander, G. B. Partridge, and R. G. Hulet, Observation of Fermi pressure in a gas of trapped atoms, *Science* **291**, 2570 (2001).

8. M. Edwards, R. J. Dodd, C. W. Clark, P. A. Ruprecht, and K. Burnett, Properties of a Bose–Einstein condensate in an anisotropic harmonic potential, *Phys. Rev. A* **53**, R1950 (1996).

9. F. Dalfovo and S. Stringari, Bosons in anisotropic traps: Ground state and vortices, *Phys. Rev. A* **53**, 2477 (1996).

10. M. L. Chiofalo, S. Succi, and M. P. Tosi, Ground state of trapped interacting Bose–Einstein condensates by an explicit imaginary-time algorithm, *Phys. Rev. E* **62**, 7438 (2000).

11. M. Holland and J. Cooper, Expansion of a Bose–Einstein condensate in a harmonic potential, *Phys. Rev. A* **53**, R1954 (1996).

12. M. M. Cerimele, M. L. Chiofalo, F. Pistella, S. Succi, and M. P. Tosi, Numerical solution of the Gross–Pitaevskii equation using an explicit finite-difference scheme: An application to trapped Bose–Einstein condensates, *Phys. Rev. E* **62**, 1382 (2000).

13. O. J. Luiten, M. W. Reynolds, and J. T. M. Walraven, Kinetic theory of the evaporative cooling of a trapped gas, *Phys. Rev. A* **53**, 381 (1996); M. Holland, J. Williams, and J. Cooper, Bose–Einstein condensation: Kinetic evolution obtained from simulated trajectories, *Phys. Rev. A* **55**, 3670 (1997); M. J. Bijlsma, E. Zaremba, and H. T. C. Stoof, Condensate growth in trapped Bose gases, *Phys. Rev. A* **62**, 063609 (2000).

14. A. Sinatra, C. Lobo, and Y. Castin, A classical field method for time dependent Bose condensed gases, *J. Phys. B* **34**, 4589 (2001); I. Carusotto and Y. Castin, An exact stochastic field method for the interacting Bose gas at thermal equilibrium, *J. Phys. B* **34**, 4589 (2001).

15. G. A. Bird, *Molecular Gas Dynamics and the Direct Simulation of Gas Flows* (Oxford Univ. Press, Oxford, 1994).

16. T. Lopez-Arias and A. Smerzi, Kinetic properties of a Bose–Einstein gas at finite temperature, *Phys. Rev. A* **58**, 526 (1998).

17. H. Wu and C. J. Foot, Direct simulation of evaporative cooling, *J. Phys. B* **29**, L321 (1996); H. Wu, E. Arimondo, and C. J. Foot, Dynamics of evaporative cooling for Bose–Einstein condensation, *Phys. Rev. A* **56**, 560 (1997).

18. L. P. Kadanoff and G. Baym, *Quantum Statistical Mechanics* (Benjamin, New York, 1962). Their formulation is in terms of the many-body single-particle Green's functions, which for a particular time ordering yield the one-body density matrix and hence the Wigner distribution function.

19. J. W. Kane and L. P. Kadanoff, Green's functions and superfluid hydrodynamics, *J. Math. Phys.* **6**, 1902 (1965).

20. A. Griffin, Conserving and gapless approximations for an inhomogeneous Bose gas at finite temperatures, *Phys. Rev. B* **53**, 9341 (1996); M. Imamović-Tomasović and A. Griffin, Coupled Hartree–Fock–Bogoliubov kinetic equations for a trapped Bose gas, *Phys. Rev. A* **60**, 494 (1999); D. A. W. Hutchinson, R. J. Dodd, and K. Burnett, Gapless finite-T theory of collective modes of a trapped gas, *Phys. Rev. Lett.* **81**, 2198 (1998).

21. E. Zaremba, T. Nikuni, and A. Griffin, Dynamics of trapped Bose gases of finite temperatures, *J. Low Temp. Phys.* **116**, 277 (1999).

22. T. Nikuni, E. Zaremba, and A. Griffin, Two-fluid dynamics for a Bose–Einstein condensate out of local equilibrium with the noncondensate, *Phys. Rev. Lett.* **83**, 10 (1999).

23. J. Wachter, R. Walser, J. Cooper, and M. Holland, Equivalence of kinetic theories of Bose–Einstein condensation, `cond-mat/0105181` (2001).

24. B. Jackson and C. S. Adams, Damping and revivals of collective oscillations in a finite-temperature model of trapped Bose–Einstein condensation, *Phys. Rev. A* **63**, 053606 (2001).

25. B. Jackson and E. Zaremba, Finite-temperature simulations of the scissors mode in Bose–Einstein condensed gases, *Phys. Rev. Lett.* **87**, 100404 (2001); B. Jackson and E. Zaremba, Dynamical simulations of trapped Bose gases at finite temperatures, *Laser Phys.* **12**, 93 (2002); J. E. Williams, E. Zaremba, B. Jackson, T. Nikuni, and A. Griffin, Dynamical instability of a condensate induced by a rotating thermal gas, *Phys. Rev. Lett.* **88**, 070401 (2002).

26. P. C. Hohenberg and P. C. Martin, Theory of Superfluid ^{4}He, *Ann. Phys. (N.Y.)* **34**, 291 (1965).

27. A. Minguzzi, S. Conti, and M. P. Tosi, The internal energy and condensate fraction of a trapped interacting Bose gas, *J. Phys.: Condens. Matter* **9**, L33 (1997).

28. M. Amoruso, A. Minguzzi, S. Stringari, M. P. Tosi, and L. Vichi, Temperature-dependent density profiles of trapped boson–fermion mixtures, *Eur. Phys. J. D* **4**, 261 (1998); M. Amoruso, I. Meccoli, A. Minguzzi, and M. P. Tosi, Collective excitations of a degenerate Fermi vapour in a magnetic trap, *Eur. Phys. J. D* **7**, 441 (1999).

29. J. M. Dawson and R. Shanny, Some investigations of non-linear behaviour in one-dimensional plasmas, *Phys. Fluids* **11**, 1506 (1968); M. Shoucri and G. Knorr, Numerical integration of the Vlasov equation, *J. Comput. Phys.* **14**, 84 (1974); C. Z. Zheng, and G. Knorr, The integration of the Vlasov equation in configuration space, *J. Comput. Phys.* **22**, 330 (1976).

30. S. I. Zaki, L. R. Gardner, and T. J. M. Boyd, A finite-element code for the simulation of one-dimensional Vlasov plasmas. I Theory, *J. Comput. Phys.* **79**, 184 (1988); A. J. Klimas and W. M. Farrell, A splitting algorithm for Vlasov simulation with filamentation filtration, *J. Comput. Phys.* **110**, 150 (1994); E. Sonnendruecker, J. Roche, P. Bertrand, and A. Ghizzo, Conservative numerical schemes for the Vlasov equation, *J. Comput. Phys.* **68**, 202 (1998); P. Dyshlovenko, Adaptive mesh enrichment for the Poisson–Boltzmann equation, *J. Comput. Phys.* **172**, 198 (2001).

31. P. B. Visscher, A fast explicit scheme for the time-dependent Schroedinger equation, *Comput. Phys.* Nov/Dec, 596 (1991).

32. R. Hockney and J. Eastwood, *Computer Simulation Using Particles* (McGraw-Hill, New York, 1981).

33. T. Pang, *An Introduction to Computational Physics* (Cambridge Univ. Press, Cambridge, UK, 1996).

34. L. Vichi, M. Inguscio, S. Stringari, and G. M. Tino, Quantum degeneracy and interaction effects in spin-polarized Fermi–Bose mixtures, *J. Phys. B* **31**, L899 (1998); L. Vichi and S. Stringari, Collective oscillations of an interacting trapped Fermi gas, *Phys. Rev. A* **60**, 4734 (1999).

35. S. Burger, F. S. Cataliotti, C. Fort, F. Minardi, M. Inguscio, M. L. Chiofalo, and M. P. Tosi, Superfluid and dissipative dynamics of a Bose–Einstein condensate in a periodic optical potential, *Phys. Rev. Lett.* **86**, 4447 (2001).

36. M. L. Chiofalo and M. P. Tosi, Josephson-type oscillations of a driven Bose–Einstein condensate in an optical lattice, *Europhys. Lett.* **56**, 326 (2001).

37. M. M. Cerimele, M. L. Chiofalo, and F. Pistella, Numerical solution of the stationary Gross–Pitaevskii equation: Tests of a combined imaginary-time-marching technique with splitting, *Nonlinear Analysis* **47**, 3345 (2001).

38. P. Pedri, L. Pitaevskii, S. Stringari, C. Fort, S. Burger, F. S. Cataliotti, P. Maddaloni, F. Minardi, and M. Inguscio, Expansion of a coherent array of Bose–Einstein condensates, `cond-mat/0108004` (2001).

39. S. Succi and F. Papetti, *An Introduction to Parallel Computational Fluid Dynamics* (Nova Science, New York, 1995).